Catal Lett (2008) 125:35–45
DOI 10.1007/s10562-008-9541-2

Unsupported NiMo Sulfide Catalysts Obtained from Nickel/Ammonium and Nickel/Tetraalkylammonium Thiomolybdates: Synthesis and Application in the Hydrodesulfurization of Dibenzothiophene

L. Álvarez · G. Berhault · G. Alonso-Nuñez

Received: 28 April 2008 / Accepted: 6 June 2008 / Published online: 24 June 2008

Abstract Ammonium and tetraalkylammonium tetrathiomolybdates impregnated with nickel nitrate were used as precursors of unsupported NiMo sulfide catalysts. The precursors were decomposed either in situ during the course of a dibenzothiophene (DBT) hydrodesulfurization (HDS) test or ex situ through sulfidation by H_2S/H_2 (15% v/v H_2S). The catalysts were characterized by thermogravimetric analysis, N_2 adsorption, scanning electron microscopy (SEM), and X-ray diffraction. Textural and catalytic properties of these NiMo catalysts were strongly influenced both by the nature of the precursor and the activation procedure. For ex-situ activated NiMo catalysts, the use of carbon-containing tetraalkylammonium thiosalts as precursors did not lead to a significant improvement in HDS activity. For in situ activated NiMo catalysts, the role of carbon is more complex. The use of tetramethyl- or tetrapropylammonium tetrathiomolybdate salts led to a poor final HDS activity while using tetrabutylammonium tetrathiomolybdate, a net increase in HDS activity was observed compared to the use of the non-carbon containing ammonium tetrathiomolybdate. This was related to the development of a mesoporous structure and to a high increase in surface area. This result is in agreement with those found previously for CoMo catalysts and confirms that tetraalkylammonium tetrathiomolybdate salts with long alkyl chains lead to Co- or Ni-promoted MoS_2-based catalysts with enhanced HDS activity if in situ activated.

Keywords NiMo · Hydrodesulfurization · Dibenzothiophene · Thiosalts · Alkylammonium

L. Álvarez (✉)
CIMAV, Miguel de Cervantes No. 120, Chihuahua C.P. 31109, Chih., Mexico
e-mail: lorena.alvarez@cimav.edu.mx

G. Berhault
Institut de Recherches sur la Catalyse et l'Environnement de Lyon, UMR 5256 CNRS Université de Lyon, 2 Avenue Albert Einstein, 69100 Villeurbanne, France

G. Alonso-Nuñez
Facultad de Ciencias, Universidad Autónoma de Baja California, Km. 106 carretera Tijuana-Ensenada, C.P. 22800 Ensenada, B.C., Mexico

1 Introduction

Due to the increasing demand concerning environmental issues, the oil industry is under pressure to provide clean fuels for vehicle transportation purposes. Therefore, attention has been focused in the last years on improving the efficiency of hydrotreating (HDT) processes to better remove heteroelements (S, N, O) responsible for the emission of pollutants. The conventional HDT processes generally use transition metal sulfides (TMS) as catalysts [1] due to their exceptional resistance to poisoning and to their catalytic performance. MoS_2 and WS_2 supported on alumina and promoted with Ni or Co are commonly used [2–5]. Textural and catalytic properties of TMS could be performed in a large extent through modifications in the nature of the precursors and procedures of synthesis [6, 7]. In this respect, thiosalts decomposition is a versatile and reproducible route for preparing MoS_2 and WS_2 catalysts with improved hydrodesulfurization (HDS) catalytic properties [8–11]. Unsupported CoMo catalysts synthesized by the decomposition of thiosalts have been claimed to exhibit higher catalytic activities than their similar counterparts obtained by classical methods of preparation [12]. An advantage of the thiosalt method is related to the fact that the decomposition into MoS_2 or WS_2 has been

reported to follow a topotactic transformation [13] since sulfur in the thiosalt compound is already bound to metal atoms in a tetrahedral coordination. Moreover, in a preceding study, we have demonstrated that the use of tetraalkylammonium thiosalts can lead to unsupported CoMo catalysts with improved textural properties and enhanced HDS activity compared to their counterparts obtained from ammonium tetrathiomolybdate (ATM) (without carbon) [14, 15]. In the present study, the use of tetraalkylammonium thiosalts has been extended to the case of unsupported NiMo catalysts. Therefore, the synthesis of nickel-promoted MoS_2 catalysts was performed by the decomposition of ammonium or tetraalkylammonium tetrathiomolybdates [$(R_4\ N)_2MoS_4$ (R = H, methyl, propyl and butyl)] impregnated with nickel nitrate. Two different methods of activation were used: an in situ method in which the precursor was directly decomposed into NiMo sulfide catalysts during the course of the dibenzothiophene (DBT) HDS run, and an ex situ method in which the precursor was initially decomposed under a H_2S/H_2 sulfiding mixture before being tested in the HDS of DBT.

2 Experimental

2.1 Synthesis of Precursors

The tetraalkylammonium tetrathiomolybdate precursors [$(R_4\ N)_2MoS_4$ (R = H, methyl, propyl and butyl)] were synthesized following the method reported elsewhere [16–18]. The tetraalkylammonium tetrathiomolybdate salts were obtained by mixing in aqueous solutions their corresponding tetraalkylammonium bromide salts with ammonium tetrathiomolybdate (ATM) at 333 K. In a second step, the required amount of $Ni(NO_3)_2 \cdot 6H_2O$ to give an atomic ratio R = Ni/(Ni + Mo) = 0.5 was added to the minimum amount of water and was dripped to an aqueous solution of the respective tetraalkylammonium tetrathiomolybdate salts to finally form an homogeneous paste. The mixture was then dried at 393 K for 2 h under N_2. The final precursors are labeled as Ni/A, Ni/M, Ni/P and Ni/B when starting, respectively, from ATM, tetramethylammonium, tetrapropylammonium, and tetrabutylammonium tetrathiomolybdate salts. These precursors are amorphous.

2.2 Activation of the Unsupported NiMo Catalysts

The catalysts were prepared following either the ex situ or the in situ activation procedure. In the ex situ method, the precursors were decomposed in a tubular furnace under a H_2S/H_2 (15 vol% of H_2S in H_2) reducing-sulfiding atmosphere at 673 K for 4 h before being tested in the HDS of DBT. In the in situ method, the precursors were directly transformed into NiMo sulfide catalysts under the experimental conditions for the HDS of DBT (see Sect. 2.4). In each case, the amount of precursor used was determined in order to obtain 1 g of catalyst for the subsequent catalytic test. The catalyst obtained from these two activation methods are hereafter labeled as follows: Ni/C_n–MoS_2, where $n = 1$, 3, or 4 accordingly to the alkyl group contained in the thiosalt precursor: methyl, propyl or butyl, respectively. The catalysts obtained from ATM are named Ni/MoS_2. All catalysts are indexed "ex situ" or "in situ" according to the method of activation.

2.3 Characterization of Catalysts

The mode of decomposition of the different precursors was studied through thermogravimetric analysis (DTA-TGA) performed on a TA Instrument SDT 2960 under a 150 mL/min flow of nitrogen (99.999% of purity). X-ray diffraction (XRD) patterns of spent catalysts were obtained on a Phillips X Pert MPD diffractometer operating at 43 kV and 30 mA and equipped with a curved graphite monochromator using Cu $K\alpha$ radiation ($\lambda = 1.54056$ Å) (it should be noted that XRD patterns of ex situ prepared samples were essentially the same before and after the HDS test). Specific surface area measurements were performed on a NOVA 1000 instrument by N_2 adsorption at 77 K using the BET isotherm while the pore-size distribution was calculated by N_2 desorption using the BJH method. Morphology determination and EDX elemental analysis were performed using a JEOL JSM5800 IV scanning electron microscope (SEM). An eBX-ZAF system was used to perform the EDX analysis. Furthermore, a very crystallized MoS_2 flake was used to deconvolute K lines of S and L lines of Mo.

All samples were evaluated in the HDS of DBT. For catalyst characterization after HDS, the spent samples were separated from the reaction solution by filtration, washed with isopropylic alcohol to remove residual hydrocarbons, and dried in air at room temperature. The ex situ prepared samples were characterized before and after HDS whereas the in situ prepared samples obtained by the direct decomposition during the DBT HDS test were characterized only after the catalytic test.

2.4 Catalytic Activity and Selectivity

The catalytic experiments were performed in a Parr batch reactor loaded with 150 mL of a 5 wt% DBT in decalin mixture. One gram of catalyst of ex-situ activated catalyst, or the appropriate amount of precursor to yield 1 g of NiMo catalyst for the in situ prepared catalysts was then placed in the reactor. The reactor was then purged with N_2, pressurized with hydrogen to 3.1 MPa, and heated up to 623 K.

The reaction mixture was kept under stirring at 600 rpm. The experiment was followed during 5 h. To determine the conversion versus reaction time, samples were collected and analyzed regularly by gas chromatography using a Perkin–Elmer auto-system gas chromatograph with a OV-17 packed column.

The HDS of dibenzothiophene occurs through two parallel pathways [19]. The main reaction products of the HDS of DBT are biphenyl (BP) formed by direct C–S bond cleavage of DBT (the so-called direct desulfurization pathway, DDS), and phenylcyclohexane (PCH) formed by the initial hydrogenation of one of the aromatic rings of DBT followed by C–S bond rupture (the hydrogenating pathway, HYD). The HYD/DDS selectivity ratio is based on the product concentration ratio (PCH/BP). It should be noted that an intermediate primary hydrogenated product, tetrahydrodibenzothiophene, is also formed along the HYD pathway. However, its concentration remained low and could be neglected when calculating the HYD/DDS ratio. Moreover, this compound is not desulfurized. The mean standard deviation for catalytic measurements was about 2.5%.

3 Results

3.1 Catalysts Preparation

The decomposition of nonpromoted precursors by in situ and ex situ methods, their characterization and activity test in the HDS of DBT have been reported elsewhere [14–18]. Nickel nitrate reacts first with tetraalkylammonium tetrathiomolybdate according to the following reaction [20], and is represented as follows:

$$\left[(CH_3)_4N\right]_2MoS_4 + Ni(NO_3)_2 \rightarrow NiMoS_4\left[N(CH_3)_4NO_3\right]_2 \quad (1)$$

$$\left[(C_3H_7)_4N\right]_2MoS_4 + Ni(NO_3)_2 \rightarrow NiMoS_4\left[N(C_3H_7)_4NO_3\right]_2 \quad (2)$$

$$\left[(C_4H_9)_4N\right]_2MoS_4 + Ni(NO_3)_2 \rightarrow NiMoS_4\left[N(C_4H_9)_4NO_3\right]_2 \quad (3)$$

The DTA–TGA curves for Ni/M, Ni/P and Ni/B precursors are reported in Fig. 1. Slight loss of water before 400 K could be observed for the different precursors (4% for Ni/M, 2% for Ni/P and Ni/B). The mode of decomposition of the nickel-promoted ammonium tetrathiomolybdate was reported elsewhere [20]. The decomposition mode of the tetraalkylammonium precursors appeared complex with multiple exothermic steps confirming previous results obtained on carbon-containing CoMo precursors [14] (Table 1). However, using mass spectrometry analyses,

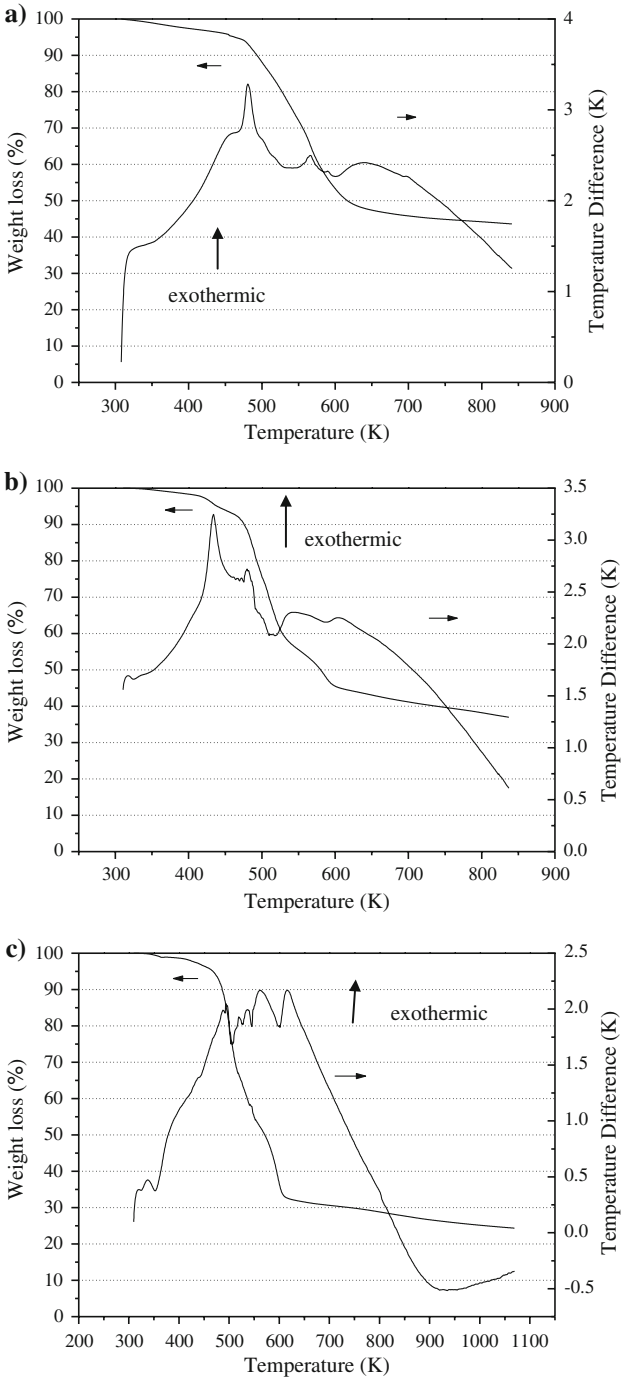

Fig. 1 DTA–TGA curves for the Ni/M (**a**), Ni/P (**b**) and Ni/B (**c**) precursors

Poisot et al. [21] have shown that during their decomposition into MoS_2, the tetraalkylammonium thiomolybdates led to the formation of trialkylamine and dialkyldisulfide compounds. This mode of decomposition might be due to a concerted S_{N2} mechanism where the α carbon of R_4N^+ is attacked by the nucleophilic sulfur atom of the MoS_4^{2-} ion. In all cases, the final stoichiometry would be $NiMoS_2$. The decomposition of the tetraalkylammonium

Table 1 DTA–TGA results of the decomposition of the Ni/M, Ni/P, and Ni/B precursors under nitrogen atmosphere

	Ni/M	Ni/P	Ni/B
Δw_{-1}, wt.% (exp) assumed as water	4	2	2
T_1 (K)	448	408	398
T_2 (K)	698	698	698
Exothermic signals	3	4	5
Δw_1, wt.% (exp)	51	58	68
Δw_1, wt % (th.)	55	64	72
Assumed loss	$2(CH_3)_3$ N + $(CH_3)_2S_2$ + $2HNO_3$	$2(C_3H_7)_3$ N + $(C_3H_7)_2S_2$ + $2HNO_3$	$2(C_4H_9)_3$ N + $(C_4H_9)_2S_2$ + $2HNO_3$
Residual, wt.% (exp)	45	40	30
Residual, wt.% (th.)	45	36	28
Assuming final product as	$NiMoS_2$	$NiMoS_2$	$NiMoS_2$

tetrathiomolybdate precursors occurs with an increasing number of exothermic peaks going from Ni/M (three peaks), Ni/P (four peaks), and Ni/B (five peaks). Moreover, increasing the alkyl chain length of the precursor results in a decrease of the onset temperature of decomposition: from 448 K for Ni/M to 408 K for Ni/P and 398 K for Ni/B.

3.2 Elemental Analysis

The S/Mo, C/Mo and Ni/(Ni + Mo) atomic ratios after the HDS reaction are reported in Table 2. Whatever the activation mode, the use of tetraalkylammonium precursors led to a higher final S/Mo ratio than when using ATM. However, the increase in the alkyl size of the precursor also progressively decreased the final S/Mo ratio from 3.0 to 2.3 for in situ activated samples and from 2.6 to 2.0 for ex situ activated catalysts. On the other hand, increasing the length of the alkyl group also decreased the C/Mo ratio from 3.6 to 1.6 for in situ activated samples and from 4.8 to 2.4 for ex situ activated samples. This situation strikingly differs from preceding results acquired on unpromoted MoS_2 [18, 21] and Co-promoted MoS_2 solids [14]. Interestingly, the ex situ activation procedure led to lower S/Mo but higher C/Mo ratios than for their in situ counterparts. Finally, the Ni/(Ni + Mo) ratio was close to 0.5 for all catalysts indicating that the metal content in the final catalyst was hardly affected by the decomposition process.

3.3 Surface Areas and Pore Size Distribution

Ex situ prepared NiMo catalysts showed much smaller surface areas than those prepared using the in situ mode of activation (Table 2) except for the $Ni/MoS_{2ex\ situ}$ catalyst in agreement with previous results [6, 10, 20]. Increasing the alkyl size of the tetraalkylammonium precursor led to a marked increase in surface area of the final NiMo catalysts for the in situ prepared samples (going from 14 m^2/g for $Ni/C_1–MoS_{2in\ situ}$ to 89 m^2/g for $Ni/C_4–MoS_{2in\ situ}$). For ex situ prepared solids, after HDS test, surface areas did not change significantly when going from $Ni/MoS_{2ex\ situ}$ to $Ni/C_4–MoS_{2ex\ situ}$ with values generally around 13–15 m^2/g (after the DBT HDS test). One exception was the $Ni/C_1–MoS_{2ex\ situ}$ catalyst with a very low surface area (3 m^2/g). Interestingly, for non-carbon containing precursors, using the in situ method of activation, the addition of Ni led to a drastic decrease in surface area from 60 m^2/g ($MoS_{2in\ situ}$)

Table 2 S/Mo and C/Mo atomic ratios after the DBT HDS test, ratio R = Ni/(Ni + Mo), and specific surface areas in m^2/g (S_{BET}) (before HDS for the ex situ samples and after HDS for both ex situ and in situ samples)

Catalyst	S/Mo	C/Mo	R	S_{BET} before HDS (m^2/g)	S_{BET} after HDS (m^2/g)
$MoS_{2in\ situ}$[a]	1.8	0.3	–	–	60
$MoS_{2ex\ situ}$[a]	1.7	0.1	–	6	8
$Ni/MoS_{2in\ situ}$	2.0	0	0.6	–	9
$Ni/MoS_{2ex\ situ}$	2.0	0.4	0.5	7	13
$Ni/C_1–MoS_{2in\ situ}$	2.8	3.6	0.5	–	14
$Ni/C_1–MoS_{2ex\ situ}$	2.6	4.8	0.5	2	3
$Ni/C_3–MoS_{2in\ situ}$	3.0	2.0	0.6	–	76
$Ni/C_3–MoS_{2ex\ situ}$	2.4	2.6	0.4	4	15
$Ni/C_4–MoS_{2in\ situ}$	2.3	1.6	0.4	–	89
$Ni/C_4–MoS_{2ex\ situ}$	2.0	2.4	0.4	10	15

[a] Results taken from [13]

to 9 m^2/g ($Ni/MoS_{2in\ situ}$). For ex situ prepared catalysts, a slight increase was observed from 8 m^2/g ($MoS_{2ex\ situ}$) to 13 m^2/g ($Ni/MoS_{2ex\ situ}$).

Figure 2 reports the adsorption–desorption isotherms for the in situ prepared catalysts. The nature of the thiosalt precursor strongly influences the porous organization of the final NiMo catalysts. Increasing the length of the alkyl chain led to a progressive development of the porosity. Type I isotherms with virtually a non-porous structure were found for $Ni/MoS_{2in\ situ}$ and $Ni/C_1–MoS_{2in\ situ}$ while $Ni/C_3–MoS_{2in\ situ}$ and $Ni/C_4–MoS_{2in\ situ}$ catalysts demonstrated type IV-like isotherms. The $Ni/C_4–MoS_{2in\ situ}$ catalyst exhibited a well-developed hysteresis loop. These results are in agreement with those previously reported for CoMo catalysts [14]. Figure 3 shows the BJH pore-size distributions of the in situ prepared catalysts. Pore size distribution curves confirmed the quasi-absence of porosity of the $Ni/MoS_{2in\ situ}$ and $Ni/C_1–MoS_{2in\ situ}$ catalysts while narrow pore size distributions centered at 38 Å diameter were found for $Ni/C_3–MoS_{2in\ situ}$ and $Ni/C_4–MoS_{2in\ situ}$ catalysts. The $Ni/C_3–MoS_{2in\ situ}$ catalyst also presents a significant contribution of smaller pores. For $Ni/C_4–MoS_{2in\ situ}$, a strong and intense peak confirmed the development of a mesoporous structure with a high surface area and also the presence of bigger pores (above 50 Å diameter).

For the ex situ prepared NiMo catalysts, the situation appeared more complex. The $Ni/MoS_{2ex\ situ}$ catalyst presents a poorly developed hysteresis loop characteristic of a low porous organization (Fig. 4) while the pore-size distribution showed only a broad peak between 20 and 40 Å in diameter (Fig. 5). For the $Ni/C_1–MoS_{2ex\ situ}$ catalyst, a quasi-absence of porosity could be observed (Fig. 5). The $Ni/C_3–MoS_{2ex\ situ}$ catalyst had the most developed porous organization with a well-defined hysteresis loop (Fig. 4) and a narrow pore size distribution (Fig. 5). However, this

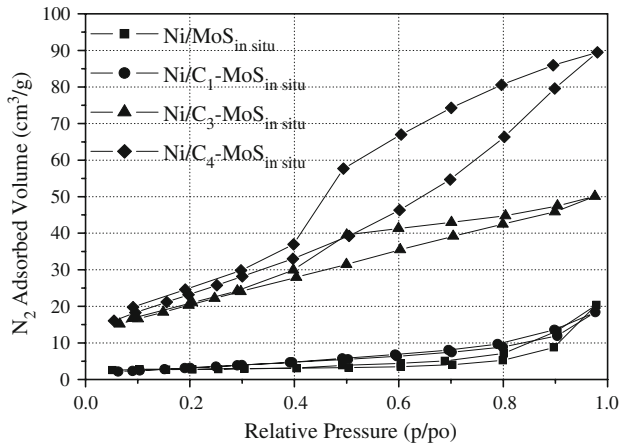

Fig. 2 N_2 adsorption–desorption isotherms for the four in situ prepared NiMo catalysts

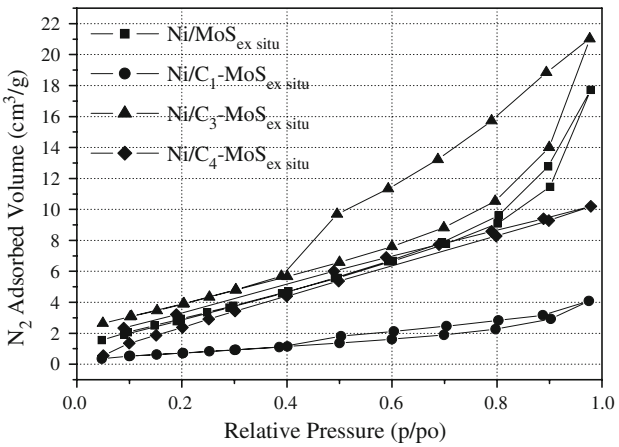

Fig. 4 N_2 adsorption–desorption isotherms for four ex situ prepared NiMo catalysts

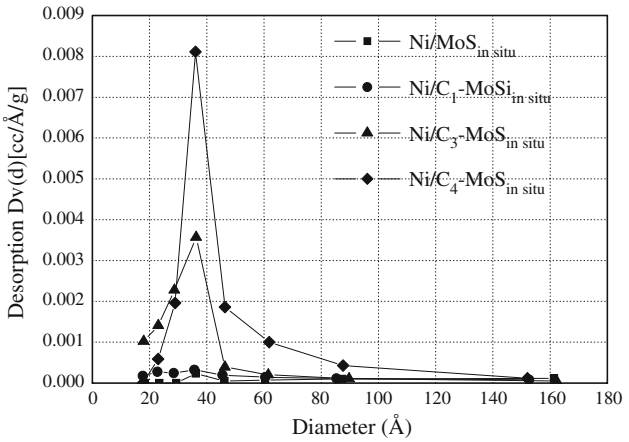

Fig. 3 Pore size distribution calculated by the BJH method for the four in situ prepared NiMo catalysts

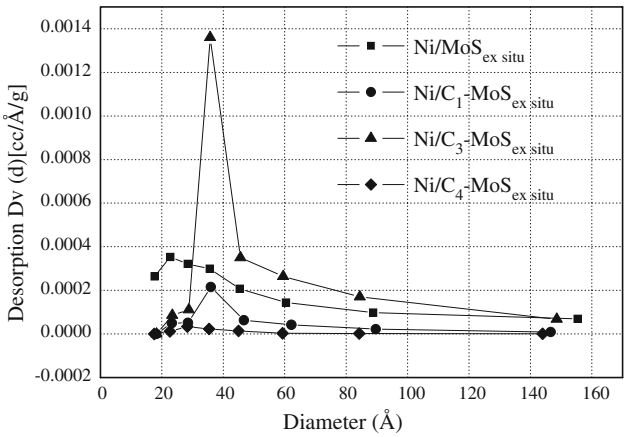

Fig. 5 Pore size distribution calculated by the BJH method for the four ex situ prepared NiMo catalysts

porous organization is still much less developed than for the Ni/C_4–$MoS_{2in\ situ}$ catalyst. This increased porosity was not confirmed when going to the Ni/C_4–$MoS_{2ex\ situ}$ case. Indeed, even if presenting a similar surface area than Ni/C_3–$MoS_{ex\ situ}$ (15 m^2/g), the Ni/C_4–$MoS_{2ex\ situ}$ catalyst demonstrated a disordered porosity characterized by the lack of a defined pore size distribution (Fig. 5).

3.4 X-Ray Diffraction

Figure 6 reports the XRD patterns obtained after the DBT HDS reaction for the in situ and ex situ prepared Ni/C_1–MoS_2 and Ni/C_4–MoS_2 catalysts. For the in situ prepared catalysts, XRD patterns present broad MoS_2 (002), (110), and (111) peaks, respectively, at $2\theta = 14°$, 34°, and 59°. MoS_2 then exhibited a poorly crystalline structure characterized by a low stacking of layers along the *c* direction [22]. Moreover, a strong scattering signal at low angles due to carbon residues could be observed particularly for the Ni/C_1–MoS_2 catalysts showing the highest C/Mo ratio (Table 2). Interestingly, both samples present additional distinct peaks due to nickel sulfide phases, Ni_9S_8 and $NiS_{1.03}$ (millerite) for Ni/C_4–$MoS_{2in\ situ}$ and NiS_2 for Ni/C_1–$MoS_{2in\ situ}$. Table 3 reports the evolution of the crystalline order lengths along both the stacking and the lateral [110] direction. When going from Ni/C_1–$MoS_{2in\ situ}$ to Ni/C_4–$MoS_{2in\ situ}$, a slight increase along stacking and basal directions could be observed suggesting a weak increase of crystallization with the use of a precursor with a longer alkyl chain length. For the ex situ prepared samples, similar XRD patterns corresponding to a MoS_2 poorly crystalline structure could be observed. However, increasing the length of the alkyl chain led to a slight decrease of the intensity of the MoS_2 (002) peak resulting in the destacking of layers (Table 3). Consecutively, the crystalline order

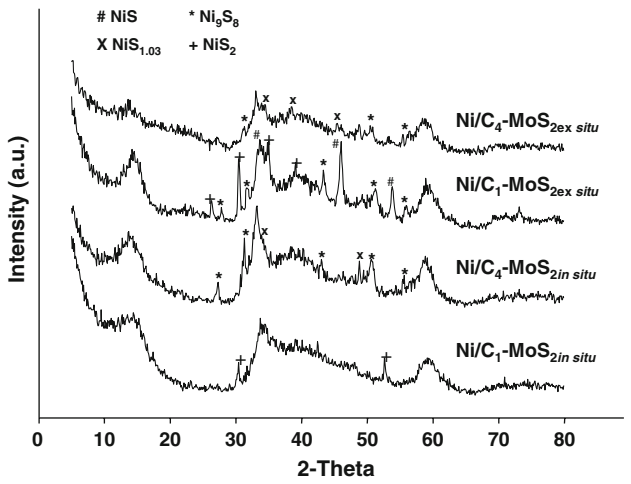

Fig. 6 XRD diffraction patterns for the Ni/C_1–$MoS_{2in\ situ}$, Ni/C_4–$MoS_{2in\ situ}$, Ni/C_1–$MoS_{2ex\ situ}$, and Ni/C_4–$MoS_{2ex\ situ}$ catalysts

Table 3 Initial rate constants and selectivity in the HDS of dibenzothiophene for the different ex situ-activated NiMo catalysts obtained from bimetallic thiosalt precursors

Catalyst	k (10^{-7} mol s^{-1} g^{-1})	HYD/DDS selectivity (after 5 h of reaction)
$MoS_{2ex\ situ}$ [a]	1.7	0.4
Ni/$MoS_{2ex\ situ}$	10.4	0.4
Ni/C_1–$MoS_{2ex\ situ}$	1.6	0.2
Ni/C_3–$MoS_{2ex\ situ}$	6.6	0.6
Ni/C_4–$MoS_{2ex\ situ}$	11.2	0.4

[a] Results taken from [13]

length moderately increases from 47 to 54 Å when going from Ni/C_1–$MoS_{2ex\ situ}$ to Ni/C_4–$MoS_{2ex\ situ}$. Like for the in situ prepared samples, distinct peaks of nickel sulfide (here, Ni_9S_8, NiS, and NiS_2 for Ni/C_1–$MoS_{2ex\ situ}$, Ni_9S_8 and $NiS_{1.03}$ for Ni/C_4–$MoS_{2ex\ situ}$) could be clearly discerned. However, for the ex situ samples, nickel sulfide peaks appeared sharper revealing a higher degree of crystallinity of the nickel sulfide phase and a more advanced nickel segregation process.

3.5 Scanning Electron Microscopy

Figure 7 shows SEM micrographs of the Ni/$MoS_{2in\ situ}$, Ni/$MoS_{2ex\ situ}$, Ni/C_4–$MoS_{2in\ situ}$ and Ni/C_4–$MoS_{2ex\ situ}$ catalysts after the HDS test. Ni/$MoS_{2in\ situ}$, Ni/$MoS_{2ex\ situ}$, and Ni/C_4–$MoS_{2ex\ situ}$ present a compact aspect. The Ni/C_4–$MoS_{2in\ situ}$ catalyst presents a slightly more open aspect. However, comparison with Co-promoted MoS_2 solids [14] confirms the lower tendency of nickel-promoted solids for the formation of highly porous network.

This result confirms that the Ni/$MoS_{2in\ situ}$, Ni/$MoS_{2ex\ situ}$, and Ni/C_4–$MoS_{2ex\ situ}$ catalysts are compact solids with low surface areas while the in situ formation of Ni-promoted MoS_2 solids using larger alkyl groups (like for Ni/C_4–$MoS_{2in\ situ}$) could lead to more open structures.

3.6 Hydrodesulfurization Activity

The curves of DBT conversion versus time of reaction are reported, respectively, Figs. 8 and 9 for ex-situ activated and in situ activated catalysts. Tables 4 and 5 summarize specific activity and selectivity results for the hydrodesulfurization of dibenzothiophene, respectively, for the ex situ activated and for the in situ activated catalysts. For comparison purposes, results about two unpromoted MoS_2 catalysts obtained by both in situ and ex situ activation procedures are also presented [14]. Catalytic activity results were influenced both by the nature of the tetraalkylammonium precursor and by the method of activation (in situ or ex situ).

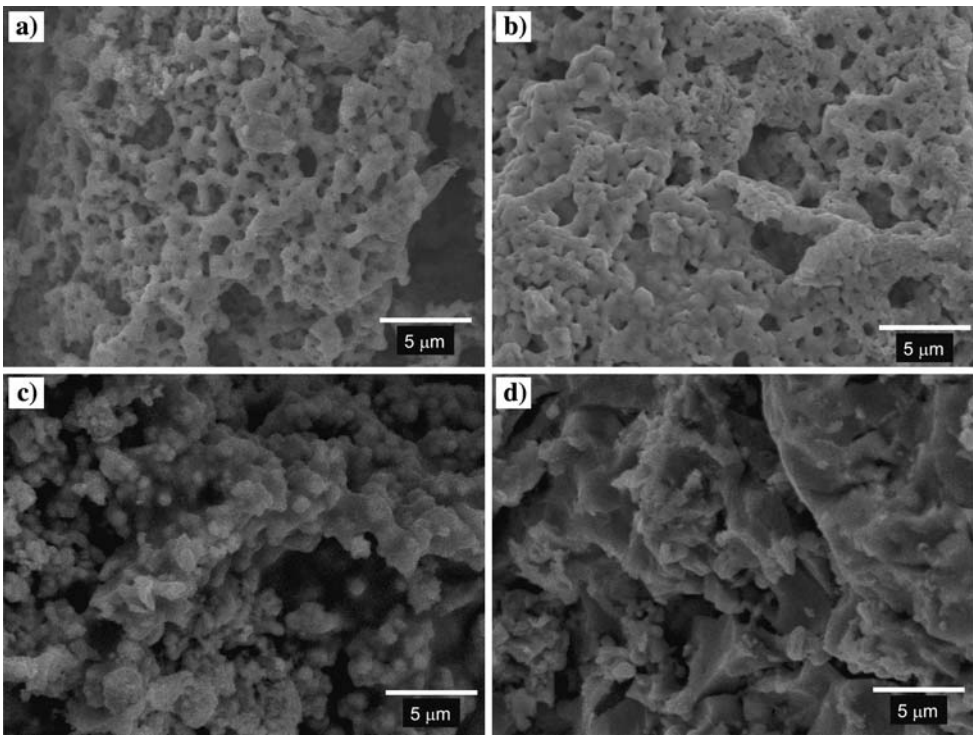

Fig. 7 SEM micrographs for the (**a**) Ni/$MoS_{2in\ situ}$, (**b**) Ni/$MoS_{2ex\ situ}$, (**c**) Ni/C_4–$MoS_{2in\ situ}$ and (**d**) Ni/C_4–$MoS_{2ex\ situ}$ catalysts

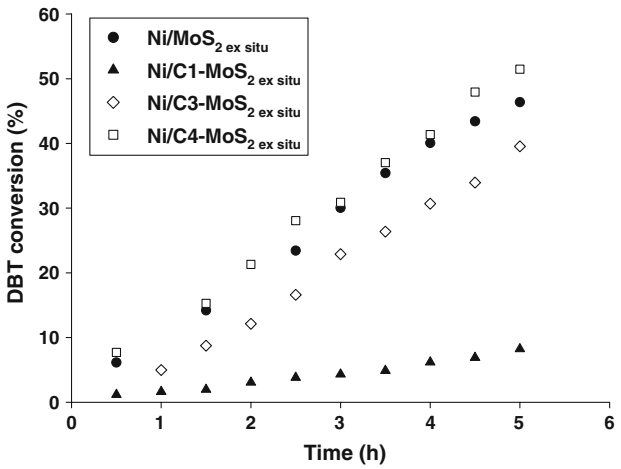

Fig. 8 Evolution of the DBT conversion versus time of reaction for the ex situ activated NiMo catalysts

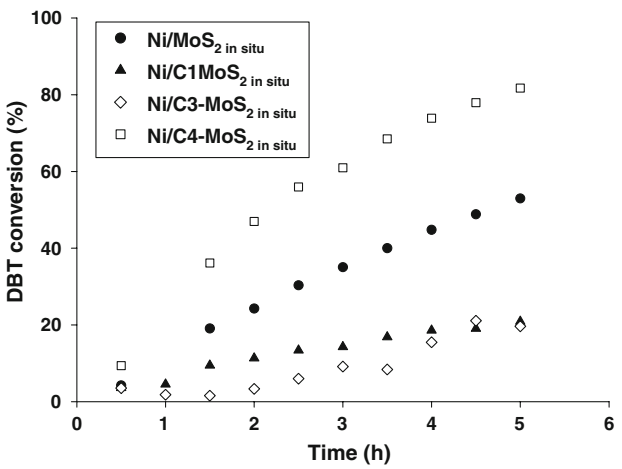

Fig. 9 Evolution of the DBT conversion versus time of reaction for the in situ activated NiMo catalysts

For the ex situ prepared catalysts, a clear synergetic effect is observed (Table 4). Indeed, the Ni/$MoS_{2ex\ situ}$ catalyst was six times as active as the $MoS_{2ex\ situ}$ reference. For the ex situ activated NiMo catalysts, Figure 8 shows a relatively linear evolution of the DBT conversion with the time of reaction confirming the absence of any deactivation phenomenon. The use of carbon-containing tetraalkylammonium precursors did not result in any improvement of the DBT HDS activity. Ni/C_4–$MoS_{2ex\ situ}$ presents similar HDS activity than the Ni/$MoS_{2ex\ situ}$ catalyst while Ni/C_3–$MoS_{2ex\ situ}$ was 35% less active than the Ni/$MoS_{2ex\ situ}$ catalyst. A surprising result concerned the Ni/C_1–$MoS_{2ex\ situ}$ catalyst. This sample presents a very low HDS activity similar to the one found for the $MoS_{2ex\ situ}$ sample revealing a complete absence of synergetic effect.

For in situ prepared catalysts, the beneficial effect of Ni on the final HDS activity was quite moderate (Table 5). This is related to an initial higher HDS activity of the $MoS_{2in\ situ}$ catalyst showing that for unpromoted MoS_2 samples, the in situ activation of the ammonium tetrathiomolybdate precursor substantially led to an improvement of the initial activity [18]. The moderate increase of activity (60%) of Ni/$MoS_{2in\ situ}$ compared to the $MoS_{2in\ situ}$ catalyst can be explained by a much lower

Table 4 Initial rate constants and selectivity in the HDS of dibenzothiophene for the different in situ-activated NiMo catalysts obtained from bimetallic thiosalt precursors

Catalyst	k (10^{-7} mol s^{-1} g^{-1})	HYD/DDS selectivity (after 5 h of reaction)
$MoS_{2in\ situ}$[a]	6.0	1.5
$Ni/MoS_{2in\ situ}$	11.9	0.7
$Ni/C_1–MoS_{2in\ situ}$	5.3	0.8
$Ni/C_3–MoS_{2in\ situ}$	2.5	0.1
$Ni/C_4–MoS_{2in\ situ}$	23.3	0.2

[a] Results taken from [13]

Table 5 Initial rate constants and selectivity in the HDS of dibenzothiophene for the different in situ-activated NiMo catalysts obtained from bimetallic thiosalt precursors

Catalyst	k (10^{-7} mol s^{-1} g^{-1})	HYD/DDS selectivity (after 5 h of reaction)
$MoS_{2in\ situ}$[a]	6.0	1.5
$Ni/MoS_{2in\ situ}$	11.9	0.7
$Ni/C_1–MoS_{2in\ situ}$	5.3	0.8
$Ni/C_3–MoS_{2in\ situ}$	2.5	0.1
$Ni/C_4–MoS_{2in\ situ}$	23.3	0.2

[a] Results taken from [13]

surface area for the nickel-promoted catalyst (9 m^2/g for $Ni/MoS_{2in\ situ}$ vs. 60 m^2/g for $MoS_{2in\ situ}$). The evolution of the DBT conversion versus time of reaction (Fig. 9) shows that like for the ex situ activated catalysts, the $Ni/MoS_{2in\ situ}$ and $Ni/C_1–MoS_{2in\ situ}$ catalysts shows a linear evolution of the DBT conversion at low DBT conversions while a slight activation was observed for $Ni/C_3–MoS_{2in\ situ}$. However, for the $Ni/C_4–MoS_{2in\ situ}$ catalyst, above 60–70% of conversion, the DBT conversion curve leveled off revealing that a first DBT order reaction was in fact achieved. Table 5 shows that the $Ni/MoS_{2in\ situ}$ catalyst was only 10% more active than $Ni/MoS_{2ex\ situ}$. Moreover, by comparison with their ex situ homologues, the in situ activated $Ni/C_1–MoS_{2in\ situ}$ and $Ni/C_3–MoS_{2in\ situ}$ catalysts did not reveal a superiority in terms of HDS activity. For these precursors with short alkyl chains, like for the ex situ prepared samples, the use of carbon-containing precursors did not improve the final HDS activity of the in situ prepared catalysts. $Ni/C_1–MoS_{2in\ situ}$ and $Ni/C_3–MoS_{2in\ situ}$ catalyst present lower activities (respectively, 5.3 and 2.5 $\times$ 10^{-7} mol/g s) than the $Ni/MoS_{2in\ situ}$ catalyst (11.9 $\times$ 10^{-7} mol/g s). In this case, the role of carbon-containing thiosalt precursors is quite negative. However, the use of a longer alkyl chain (i.e., a butyl group) led to a different result. For this precursor, the final HDS activity of the $Ni/C_4–MoS_{2in\ situ}$ was twice as high as for $Ni/MoS_{2in\ situ}$. This result is in agreement with preceding studies showing the beneficial effect of using thiosalt precursors with long alkyl chain for preparing active HDS CoMo catalysts [15].

For in situ prepared catalysts, selectivity results demonstrate that all Ni-containing samples present lower HYD/DDS ratios than for the $MoS_{2in\ situ}$ reference as expected for Ni-promoted MoS_2 catalysts [23–26]. This effect is particularly pronounced using tetraalkylammonium thiosalt precursors with longer alkyl chains ($Ni/C_3–MoS_{2in\ situ}$ and $Ni/C_4–MoS_{2in\ situ}$). In this case, the HYD/DDS ratio was only 0.1–0.2 vs. 0.7–0.8 for $Ni/MoS_{2in\ situ}$ and $Ni/C_1–MoS_{2in\ situ}$ showing that very DDS selective catalysts were obtained for $Ni/C_3–MoS_{2in\ situ}$ and $Ni/C_4–MoS_{2in\ situ}$. For ex situ prepared catalysts, no clear tendency can be discerned comparing HYD/DDS ratios, all the samples presenting ratios comprised between 0.2 and 0.6.

4 Discussion

The use of tetraalkylammonium tetrathiometallate precursors to synthesize promoted or non-promoted MoS_2 (or WS_2) catalysts has been extensively studied [14–18, 20, 21, 27–35]. Results clearly indicates that, depending on the mode of activation (in situ or ex situ), the textural and catalytic properties of MoS_2-based catalysts can be strongly modified. For unsupported MoS_2 catalysts, using the in situ method of activation, the use of carbon-containing precursors strongly increased the surface area of the as-formed MoS_2 catalysts compared to the ATM precursor (up to 329 m^2/g using the tetrapentylammonium precursor) while the HDS activity did not increase [18]. However, selectivity for the HDS of DBT was shifted to the DDS route due to confining effects inside the mesoporous structure [18].

This situation differs from the one observed for Co-promoted MoS_2 catalysts. A beneficial effect on the final HDS activity of carbon-containing tetraalkylammonium precursors was indeed clearly observed for CoMo catalysts prepared using the in situ method of activation [14, 15, 33]. $Co/C_4–MoS_{2in\ situ}$ catalyst was twice more active than $Co/MoS_{2in\ situ}$ (17.3 $\times$ 10^{-7} mol g^{-1} s^{-1} vs. 9.4 $\times$ 10^{-7} mol g^{-1} s^{-1}). Moreover, like for MoS_2 catalysts, surface areas reached high values (up to 320 m^2/g for $Co/C_6–MoS_{2in\ situ}$). On the other hand, CoMo catalysts prepared by the ex situ method of activation present low surface areas and low HDS activities. This beneficial role of C for in situ activated cobalt-promoted MoS_2 catalysts was then assumed to be partly related to the formation of a sulfocarbide surface active phase [36–38]. The formation of a sulfocarbide active phase was confirmed recently using DFT calculations considering either carburization of molybdenum sulfide [39] or sulfidation of molybdenum carbides [40].

For WS_2 catalysts, the use of carbon-containing precursors did not result in improved HDS activity for NiW catalysts, $Ni/WS_{2in\ situ}$ being even slightly more active than its NiW counterparts synthesized using tetraalkylammonium

tetrathiotungstate precursors [41]. Contrary to MoS_2, the use of carbon-containing tetraalkylammonium precursors strongly increased the rate of crystallization of WS_2 leading to bigger and more stacked particles. Moreover, carbon led to a segregation of nickel sulfide limiting the synergetic effect of nickel. This segregation effect was ascribed to a limited accommodation of Ni on WS_2 slabs due to the increased crystallization rate of tungsten sulfide and/or to a physical blocking by carbon of nickel promoting atoms unable to interact with WS_2.

To determine, if for Ni-promoted systems, carbon could block the migration of Ni atoms toward the edge sites of MeS_2 (Me = Mo or W), we have studied herein the influence of tetraalkylammonium precursors (and therefore the influence of carbon) on the formation of NiMo catalysts. In this case, like for MoS_2 or CoMo catalysts, carbon is not expected to influence the crystallization rate of the molybdenum sulfide phase as shown below.

Like for NiW catalysts [41], the tetraalkylammonium precursors exhibit a complex mode of decomposition between 398 and 698 K corresponding to multiple transition steps (Table 1). Similarly, for ex situ activated samples, SEM micrographs showed the formation of a compact structure similar to the one reported for NiW samples (Fig. 7) [42]. However, comparison between NiMo and NiW catalysts obtained by the decomposition of tetraalkylammonium precursors cannot be extended to all the different precursors used showing that a physical blocking of nickel promoting atoms cannot be considered for NiMo catalysts contrary to the NiW case. For NiMo catalysts, the use of carbon-containing thiosalts did not systematically lead to low HDS active catalysts.

For ex situ activated catalysts, the use of tetraalkylammonium tetrathiomolybdate salts did not improve the final HDS activity (Table 4). A similar result was found for CoMo catalysts [14]. This is quite expected if considering elemental analysis, BET surface area, XRD and SEM results. First of all, the ex situ activated catalysts systematically present higher C/Mo and lower S/Mo ratios than their in situ activated counterparts (Table 2). These higher C/Mo ratios were also combined with a low surface area only reaching 15 m^2/g after DBT HDS test. This low surface area results from the formation of a compact agglomerated structure as revealed by the SEM study (Fig. 7). This effect was already observed for MoS_2 [17], NiW [41], CoW [43], and CoMo [13] catalysts and seems to be directly related to the ex situ method of activation based on the decomposition under H_2S/H_2 of the thiosalt precursor before the HDS test. This mode of activation results in a collapsed structure with a low porosity (Fig. 5) and also with a higher degree of segregation of nickel into nickel sulfides as confirmed by XRD (Fig. 6). This is particularly true for the $Ni/C_1–MoS_{2ex\ situ}$ which presents strong reflections of different nickel sulphide phases (Ni_9S_8, NiS, NiS_2). Moreover, the use of a longer alkym chain in the precursor only led to the formation of nickel sulphide phases with S/Ni ratio close to 1. This higher degree of segregation led to a partial loss of Ni promotion (Table 3). Indeed, ex situ prepared catalysts were not very active and selectivity results did not vary in a large extent when comparing unpromoted and Ni-promoted solids.

This situation strikingly differs from the one observed for in situ activated thiosalt precursors for which the length of the alkyl chain length of the tetraalkylammonium tetrathiomolybdates directly influences the textural and morphological properties of the final MoS_2-based catalysts. For the $Ni/MoS_{2in\ situ}$ and $Ni/C_1–MoS_{2in\ situ}$ precursors, the situation did not really differ from the one found for their ex situ activated homologues. Nitrogen adsorption studies (Fig. 2) showed the formation of type I isotherms leading to solids with low surface areas (13–14 m^2/g). This led to a moderate increase in HDS activity for $Ni/MoS_{2in\ situ}$ compared to $MoS_{2in\ situ}$. For the tetraalkylammonium $Ni/C_1–MoS_{2in\ situ}$ precursor, the situation was even worse since a very high amount of carbon in excess was generated during the in situ decomposition. In this case, this excess carbon led to a lower HDS activity compared to $Ni/MoS_{2in\ situ}$. However, selectivity results showed a HYD/DDS ratio of 0.7 similar to the $Ni/MoS_{2in\ situ}$ catalyst and lower than for unpromoted $MoS_{2in\ situ}$. Since the promotion by Co or Ni is known to increase the C–S bond cleavage rate [26], this higher DDS selective character suggests that the nickel atoms were still involved in a promoted NiMo phase and that the segregation into nickel sulfide observed on XRD patterns (Fig. 6) only concerned a minor proportion of the nickel atoms. The excess carbon then probably blocked the active sites of the NiMo phase but did not avoid the migration of Ni atoms to the edges of MoS_2 layers. It should be underlined that another way to limit the segregation of nickel into nickel sulfide can be provided through the use of precursors containing chelating ligands like diethylenetriamine [44] which are known to retard the sulfidation of Ni and favor its accommodation on MoS_2 slabs [45, 46].

An intermediate case was provided by the $Ni/C_3–MoS_{2in\ situ}$ catalyst. Contrary to the $Ni/C_1–MoS_{2in\ situ}$ catalyst, the $Ni/C_3–MoS_{2in\ situ}$ sample showed a type IV isotherm with a moderately developed hysteresis loop (Fig. 2) and porosity (Fig. 3). Its surface area, therefore, increased up to 76 vs. 14 m^2/g for $Ni/C_1–MoS_{2in\ situ}$. However, the HDS activity remained quite low showing that the development of a mesoporous structure with high surface area was still insufficient to counterbalance the blocking of active sites by excess carbon. An interesting feature to underline was related to the selectivity results for the $Ni/C_3–MoS_{2in\ situ}$ catalyst. The HYD/DDS ratio was

quite low (0.1) showing an enhanced DDS selective character. This point will be further discussed below.

When going from tetrapropylammonium to tetrabutylammonium precursors, the effect of the alkyl chain length on the textural and morphological properties was more evident. For the Ni/C_4–$MoS_{2in\ situ}$ catalyst, a type IV isotherm with a very well developed hysteresis loop was found (Fig. 2) leading to an enhanced porosity (Fig. 3) and a higher surface area (89 m^2/g) (Table 2). Moreover, this catalyst showed the lowest C/Mo ratio (1.6) suggesting a moderate effect of excess carbon. These improved textural properties had a direct effect on the final HDS activity which was twice as high as for the Ni/$MoS_{2in\ situ}$ catalyst. The segregation into nickel sulfide observed on the XRD pattern (Fig. 6) therefore only concerns a minor proportion of nickel. Moreover, the addition of the hydrogenating Ni promoter apparently favored the hydrogenation of the resulting carbonaceous fragments present on the catalysts and their elimination. The efficiency of such elimination seems to be related to the development of a porous structure: compact carbonaceous structure apparently blocks the accessibility of hydrogen to the nickel promoting atoms: the highest C/Mo ratio (4.8) is observed for the lowest surface area (3 m^2/g, Ni/C_1–$M_{oS2ex\ situ}$) while the lowest C/Mo ratio obtained from carbon-containing precursors (1.6, Ni/C_4–$MoS_{2in\ situ}$) corresponds to the highest surface area (89 m^2/g). This result is in agreement with previous results found for CoMo catalysts, i.e. a well-developed mesoporous organization led to high surface area and highly HDS active unsupported catalysts [14, 15].

A direct role of carbon on the morphological and textural properties of MoS_2-based catalysts was therefore observed for both non-promoted and Co- or Ni-promoted catalysts. However, the role of carbon is more complex. The effect of carbon is not only limited to a negative influence of excess carbon blocking active sites of MoS_2-based catalysts. In previous studies [37, 38], it was shown that carbon can also play a beneficial structural role by forming surface carbide-like entities at the edges of MoS_2 layers under typical HDS conditions as confirmed by NEXAFS studies [47]. This structural role cannot be ruled out in the present case even if differentiation between a structural or a morphological role is not possible herein. However, the fact that better textural properties led to substantial improved HDS activity for CoMo and NiMo catalysts and not for MoS_2 suggests that the structural role of carbon could have a bigger effect for promoted systems as expected from the study by Berhault et al. [38]. This effect could be related to the interaction of dialkyldisulfides formed during the decomposition of the tetraalkylammonium precursors (cf. Table 1) with the MoS_2 active phase. The role of carbon could also be related to a stabilizing effect maintaining a high degree of dispersion [48, 49].

The Ni/C_4–$MoS_{2in\ situ}$ catalyst also presents a very high DDS selectivity since its HYD/DDS ratio was quite low (0.2) like for the Ni/C_3–$MoS_{2in\ situ}$ catalyst. This result was in fact already observed previously for MoS_2 catalysts obtained in a similar way [18]. In the Rim-Edge model developed by Daage and Chianelli [50], two types of sites are located on stacked MoS_2 layers: the "rim" sites on top and bottom layers able both to hydrogenate and cleave C–S bonds and "edge" sites located on internal layers and only able to cleave C–S bonds. The differentiation between these two kinds of sites was related to steric hindrance on "edge" sites hampering the η_6 adsorption of the DBT molecule, prerequisite for the hydrogenation step. In the present case, the stacking degree (given by the FWHM value of the MoS_2 (002) peak at $2\theta = 14°$) of Ni/C_1–$MoS_{2in\ situ}$ and Ni/C_4–$MoS_{2in\ situ}$ catalysts did not differ really as shown in Fig. 6. This also ruled out an effect of carbon on the crystallization rate of MoS_2 and shows that the Rim-Edge alone cannot satisfactorily explain such a high DDS selectivity for Ni/C_3–$MoS_{2in\ situ}$ and Ni/C_4–$MoS_{2in\ situ}$ without considering the textural properties of these catalysts. In fact, as already observed for MoS_2 catalysts [14, 15, 18], the high DDS selectivity would be a direct consequence of the mesoporous character of these catalysts leading to confinement effects restricting the sterically demanding η_6 adsorption on "rim" sites of MoS_2 layers located inside mesoporous cavities.

5 Conclusion

NiMo sulfide catalysts were prepared by in situ or ex situ decomposition of nickel promoted tetraalkylammonium tetrathiomolybdate precursors (R = C_1, C_3, C_4) and compared to NiMo catalysts obtained from nickel/ammonium tetrathiomolybdate in order to determine the influence of carbon on the textural and catalytic properties of unsupported NiMo catalysts. The ex situ method of activation led to low surface area and non (or low) porous solids with high amount of carbon resulting in low HDS activities. For in situ activated catalysts, the alkyl group in the tetraalkylammonium precursor had a direct impact on morphological and catalytic properties. Increasing the length of the alkyl chain from C_1 to C_4 led to solids with type IV isotherms and high surface areas. Therefore, while the Ni/C_1–$MoS_{2in\ situ}$ catalyst showed a depleted HDS activity, the Ni/C_4–$MoS_{2in\ situ}$ catalyst exhibits a very high HDS activity (twice as high as than for Ni/$MoS_{2in\ situ}$) and a very high DDS selectivity due to an enhanced mesoporous network and a high surface area.

Acknowledgments The authors thank the technical support of Carlos Ornelas, Daniel Lardizabal, Armando Reyes and Wilberth

Antunez in the characterization of all samples, and the financial support No. 40118-Y from CONACYT.

References

1. Berhault G, Chianelli RR (2002) In: Horvath I (ed) Encyclopedia of catalysis. Wiley, New York, p 694
2. Chianelli RR (1984) Catal Rev Sci Eng 26:361
3. Weisser O, Landa S (1973) Sulfide catalysts: their properties and application. Pergamon Press, Oxford
4. Topsøe H, Clausen BS, Massoth FE (1996) Hydrotreating catalysis—catalysis, science and technology, vol 11. Springer-Verlag, Berlin
5. Breysse M, Berhault G, Kasztelan S, Lacroix M, Maugé F, Pérot G (2001) Catal Today 66:15
6. Frety R, Breysse M, Lacroix M, Vrinat M (1984) Bull Soc Chim Belg 93:663
7. Ramanathan K, Weller S (1985) J Catal 95:249
8. Candia R, Clausen BS, Topsøe H (1982) J Catal 77:564
9. Hagenbach G, Courty P, Delmon B (1973) J Catal 31:264
10. Zdrazil M (1988) Catal Today 3:269
11. Wilkinson K, Merchan MD, Vasudevan PT (1997) J Catal 171:325
12. Fuentes S, Diaz G, Pedraza F, Rojas H, Rosas N (1988) J Catal 113:535
13. Frommell E, Diehl J, Tamilia J, Pollack S (1991) In: Proceedings of 12th North American Catalysis Society Meeting, Lexington, KY, PD-38
14. Alvarez L, Espino J, Ornelas C, Rico JL, Cortez MT, Berhault G, Alonso G (2004) J Mol Catal A Chem 210:105
15. Nava H, Ornelas C, Aguilar A, Berhault G, Fuentes S, Alonso G (2003) Catal Lett 86:257
16. Alonso G, Aguirre G, Rivero IA, Fuentes S (1998) Inorg Chim Acta 274:108
17. Alonso G, Berhault G, Chianelli RR (2001) Inorg Chim Acta 316:105
18. Alonso G, Berhault G, Aguilar A, Collins V, Ornelas C, Fuentes S, Chianelli RR (2002) J Catal 208:359
19. Whitehurst DD, Isoda T, Mochida I (1998) Adv Catal 42:345
20. Pedraza F, Fuentes S (2000) Catal Lett 65:107
21. Poisot M, Bensch W, Fuentes S, Alonso G (2006) Thermochim Acta 444:35
22. Perez De la Rosa M, Texier S, Berhault G, Camacho A, Yacaman MJ, Mehta A, Fuentes S, Montoya JA, Murrieta F, Chianelli RR (2004) J Catal 225:288
23. Kabe T, Ishihara A, Zhang Q (1993) Appl Catal A Gen 97:L1
24. Meille V, Schulz E, Lemaire M, Vrinat M (1997) J Catal 170:29
25. Michaud P, Lemberton JL, Pérot G (1998) Appl Catal A Gen 169:343
26. Bataille F, Lemberton JL, Michaud P, Pérot G, Vrinat M, Lemaire M, Schulz E, Breysse M, Kasztelan S (2000) J Catal 191:409
27. Eltzner W, Breysse M, Lacroix M, Vrinat M (1986) Polyhedron 5:203
28. Alonso G, Petranovskii V, Del Valle M, Cruz-Reyes J, Licea-Claverie A, Fuentes S (2000) Appl Catal A Gen 197:87
29. Alonso G, Del Valle M, Cruz J, Licea-Claverie A, Petranovskii V, Fuentes S (1998) Catal Today 43:117
30. Alonso G, Del Valle M, Cruz J, Licea-Claverie A, Petranovskii V, Fuentes S (1998) Catal Lett 52:55
31. Brito J, Ilija M, Hernandez P (1995) Thermochim Acta 256:325
32. Walton RI, Hibble SJ (1999) J Mater Chem 9:1347
33. Trakarnpruk W, Seentrakoon B (2007) Ind Eng Chem Res 46:1874
34. Yoneyama Y, Song C (2002) Energy Fuels 16:767
35. Genuit D, Afanasiev P, Vrinat M (2005) J Catal 235:302
36. Pecoraro TA, Chianelli RR (1985) US Patent 4,528,089
37. Berhault G, Mehta A, Pavel AC, Yang J, Rendon L, Yacaman MJ, Cota L, Duarte A, Chianelli RR (2001) J Catal 198:9
38. Berhault G, Cota L, Duarte A, Mehta A, Chianelli RR (2002) Catal Lett 78:81
39. Wen XD, Cao Z, Li YW, Wang J, Jiao H (2006) J Phys Chem B 110:23860
40. Ping L, Rodriguez JA, Muckerman JT (2005) J Mol Catal A Chem 239:116
41. Poisot M, Bensch W (2007) Thermochim Acta 453:42
42. Alonso G, Espino J, Berhault G, Alvarez L, Rico JL (2004) Appl Catal A Gen 266:29
43. Espino J, Alvarez L, Ornelas C, Rico JL, Fuentes S, Berhault G, Alonso G (2003) Catal Today 90:71
44. Poisot M, Bensch W, Fuentes S, Ornelas C, Alonso G (2007) Catal Lett 117:43
45. Coulier L, De Beer VHJ, van Veen JAR, Niemantsverdriet JW (2001) J Catal 197:26
46. Cattaneo R, Rota F, Prins R (2001) J Catal 199:318
47. Kelty SP, Berhault G, Chianelli RR (2007) Appl Catal A Gen 322:9
48. Genuit D, Afanasiev P, Vrinat M (2005) J Catal 235:302
49. Bezverkhyy I, Afanasiev P, Lacroix M (2005) J Catal 230:133
50. Daage M, Chianelli RR (1994) J Catal 149:414